Mining, Metallurgy & Exploration (2023) 40:529–541
https://doi.org/10.1007/s42461-023-00733-1

REVIEW

Modified Design of Pillar Based on Estimated Stresses and Strength of Pillar in an Underground Limestone Mine

Aman Soni[1] · Juan J. Monsalve[1] · Richard Bishop[1] · Nino Ripepi[1]

Received: 21 March 2022 / Accepted: 3 January 2023 / Published online: 30 January 2023

Abstract

The design and strength of pillars are important parameters while implementing the room-and-pillar mining method in a limestone mine. The process becomes complex with the presence of the karst voids which are frequent phenomena in a carbonate rock formation. The karst system is a network of cavities that along with an omnipresent fracture network may lead to ground control issues in a limestone mine. The objective of this study is to provide a safe and reliable alternative design for a pillar in a case study mine for safe and efficient ore recovery. This research is a continuation of a previous study aimed at studying the effect of karst void on the strength of the same limestone pillar. It was assessed from the calculated pillar strength and the estimated redistributed stresses that the pillar is capable of countering more stress than is currently imparted on it. Numerical modeling studies combining in situ stress determination and excavation sequencing were used to estimate the existing stresses on the pillar. Different possibilities of modification to existing pillar design were simulated using Distinct-Element Modeling (DEM) to determine a better design. Discrete fracture networks (DFNs) were included to imitate the effect of the presence of discontinuities. An effort is also made to understand the variation of pillar strength with height for karst-affected pillars using two different constitutive models. This study serves as a preliminary investigation in terms of improving the future design of pillars and also while recovering old pillars prone to karst formation.

Keywords Pillar strength · Pillar design · Karst · 3DEC · DEM · DFN · Secondary recovery

1 Introduction

Underground operations for mining limestone deposits experience a greater number of reported incidents compared to surface operations. To manage ground control issues during complex underground operations, special attention has to be given during mine design for long-term planning. As a part of short-term planning, while undergoing development or stope extraction, operators have to adjust pillar design to counter local stability issues as well as for efficient ore recovery. At present, 110 underground stone mines are operating in the USA, the majority of which are room-and-pillar mines (NIOSH, 2021). Compared to flat deposits, ground stability management gets more complex in a dipping room-and-pillar mine.

The majority of underground limestone deposits have extensive fracture networks. Over a while, erosion of carbonate deposits due to groundwater flow through the fracture networks leads to the formation of cavities called karsts. [11]. The karstic features including clay-filled voids, dolines, and conduits are usually connected with an aquifer and tend to increase groundwater flow into the mine [14]. The disruption of mining operations caused by karsts and the potential ground control measures have been documented by many researchers [8, 10, 15]. Non-destructive geophysical surveys, including Ground-Penetrating Radar (GPR) surveys, are often conducted to detect these cavities as a suitable approach for detecting these geological anomalies in advance of excavation development [7].

Preventing pillar failure and maintaining local and global stability are the two cardinal factors in deciding pillar design. Some major mine disasters, including the Crandall Canyon mine disaster in 2007, are proof enough that when going for economic recovery, global and local stability should be a primary concern for operators [12].

✉ Aman Soni
amansoni@vt.edu

[1] Mining and Minerals Engineering, Virginia Polytechnic Institute & State University, Blacksburg, VA, USA

Geomechanical models, along with field instrumentation data analysis, play an important role in the evaluation of the structural behavior of pillars and the effect of stresses. This becomes particularly important in limestone deposits embedded with karsts, due to the variability of fractured rock mass and their pattern and orientation to in situ stresses [1].

This paper evaluates the various modifications to the design of a pillar (designated Pillar-X) with the presence of a karst void in it. A previous study was conducted [16], which determined the effect of karst void on the strength of Pillar-X. Using the estimated pillar strength and the redistributed stresses, it was inferred that the pillar is capable of bearing more load than it is currently exposed to. Previously, at the case study mine, investigative work was conducted to detect the shape and volume of karst void(s) in the Pillar-X with the help of a 3-dimensional GPR survey [2]. The case study mine has frequently experienced ground control issues such as roof and rib failures because of karstic features in the past. The size of Pillar-X was left wider at the base and shorter in height than the usual pillar dimensions of 24.5 m × 24.5 m × 30.5 m to counter any potential instability issue because of karst in it. The paper also discusses the background of the research from the previous study showing the potential of modifying the height of Pillar-X. For this purpose, a rough schematic of the ideal mine layout along with the original excavation sequence is numerically simulated using FLAC-3D to estimate the existential stress distribution on and around the pillar. Because of the presence of a complex discontinuity network in the mine, discrete element modeling (DEM) was used to simulate the rock mass as a discontinuous media for measuring pillar strength. For this purpose, 3-dimensional numerical modeling tool 3DEC was used along with discrete fracture networks (DFNs) to replicate the presence of complex discontinuities. Since all of the discontinuities cannot be mapped inside Pillar-X, DFNs become the closest possible representation to simulate the virtual network system compared to a real-world joint network. The physico-mechanical properties used were measured by the mining company and verified using laboratory testing. The joint properties were obtained based on the work performed by Monsalve et al. [13] for the same case study mine. Pillar-X's strength was tested by modifying the height of the pillar model in a stepwise manner by increasing 10 ft or 3.05 m at a time. Since ground control measures were employed after the detection of karst in the pillar, changing the base dimensions of the pillar would present a difficult excavation scenario. Models with a subsequent increase in height were tested until the factor of safety for the pillar was above or equal to a value of 1.5 [9]. For each scenario, the pillar model was analyzed for its strength based on a constant axial compressive velocity applied to it. The analysis also characterizes the significant reduction in the pillar strength in the different scenarios, each with increased height. The paper also discusses the best possible height scenario to the original square-base model of the pillar with the same improved height. This would compare to the situation where the decision to change the design of the pillar by the mine operator was better than the original design. The paper discusses the importance of short-term planning in underground stone mines for pillar design in the presence of karsts for efficient recovery as well as maintaining pillar stability.

2 Background

2.1 Original Pillar Design

The case study mine is in a limestone deposit that hosts an extensive network of interconnected karst voids. The room-and-pillar mining method is employed to mine a 30-m-thick orebody that dips at approximately 30° from the horizontal. The footwall and hanging wall tunnels which are approximately 8-m tall and 12.8-m wide are separated by 24.5 m × 24.5 m × 30.5 m rectangular pillars left after complete extraction from the stoping.

The pillar for which iterative simulations are conducted, named Pillar-X for this study, is shown in Fig. 1. Figure 2 shows the positioning of karst cavities inside the pillar as determined using the GPR survey [2]. The excavation around Pillar-X was discontinued as a result of the opening up of the karst void with unconsolidated clayey material spilling out of the cavity. When the voids were discovered, the mine management decided to leave the pillar with bigger dimensions to counter local instability issues. Also, stope in the subsequent level was not excavated to provide extra stability to Pillar-X (Fig. 3).

The spillage of clayey-rocky material from the pillar required the mine management to employ ground support measures such as mesh pinned up with a steel strap.

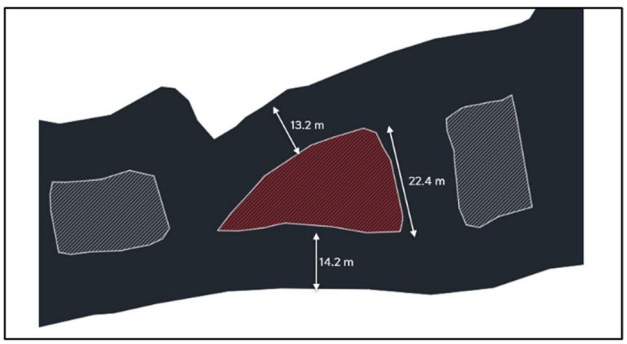

Fig. 1 Schematic view of Pillar-X next to original design pillars

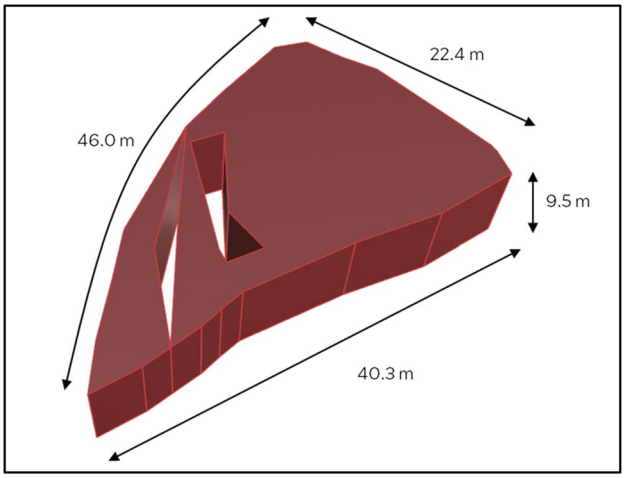

Fig. 2 Modified dimensions of Pillar-X along with karst voids located in it

Fig. 3 Excessive spillage of clayey material and water from an open karst void [5]

Fig. 4 Ground support measures taken around Pillar-X [4]

Furthermore, grouting was done as a ground control measure to prevent a further outflow of clayey sludge. Figure 4 shows the ground controls measures taken around Pillar-X.

2.2 Pillar Strength Determination

A previously completed study simulates the presence of karst voids in Pillar-X and estimates its strength for various scenarios [16]. Different results were obtained when the strength of Pillar-X is tested for three scenarios of varying karst cavity volume in increasing order. The study was an important preliminary research to understand the behavior of the original pillar design and local stability for future pillar design operations. It was also important to research the aspect of using numerical modeling to assess local stability using DFNs with the presence of karsts. The following conclusions were drawn from this study:

- The karst voids, filled with rocky-clayey material, interact with the immediate roof and fracture network resulting in a reduction of pillar strength.
- Stress was applied to the top and bottom face of the pillar in the form of constant velocity in 3DEC. Deterioration of the pillar models was observed with increasing compressive stresses.
- The solid pillar model with no voids failed at ~ 54 MPa showing the highest strength amongst all the three scenarios.
- For scenario 2, the pillar model with the suggested karst voids yielded and failed at ~ 43 MPa. This indicated a significant reduction in strength due to the presence of a karst cavity inside. Figure 5a and b shows the stress vs strain plot for a deteriorating Elastic model with increasing compressive stress.
- In scenario 3, the pillar model was simulated with the biggest karst void. It showed the least strength of all the models with a failure stress level of ~ 28 MPa. Also, the pillar model showed extensive deterioration compared to the previous scenarios Fig. 6a and b shows the stress vs strain plot for a deteriorating Mohr–Coulomb model with increasing compressive stress.
- The research suggested that with increasing void volume inside the pillar, the ability of the pillar to withstand higher stresses decreases.
- Based on the ground observations and the simulation results, it was concluded that scenario 2 resembled the current ground conditions and how the karst cavity opened when the surrounding area was mined out. Figure 7 shows a comparison of pillar strength for simulating Elastic and Mohr–Coulomb rock mass state.

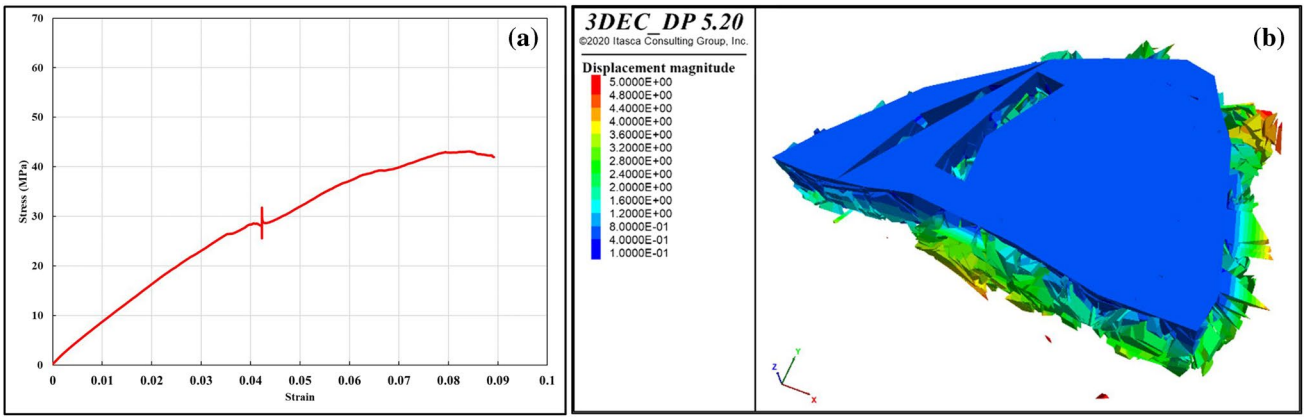

Fig. 5 **a** Stress vs strain plot for Elastic pillar model (left); **b** displacement magnitude and deterioration of the Elastic pillar model at its strength (right)

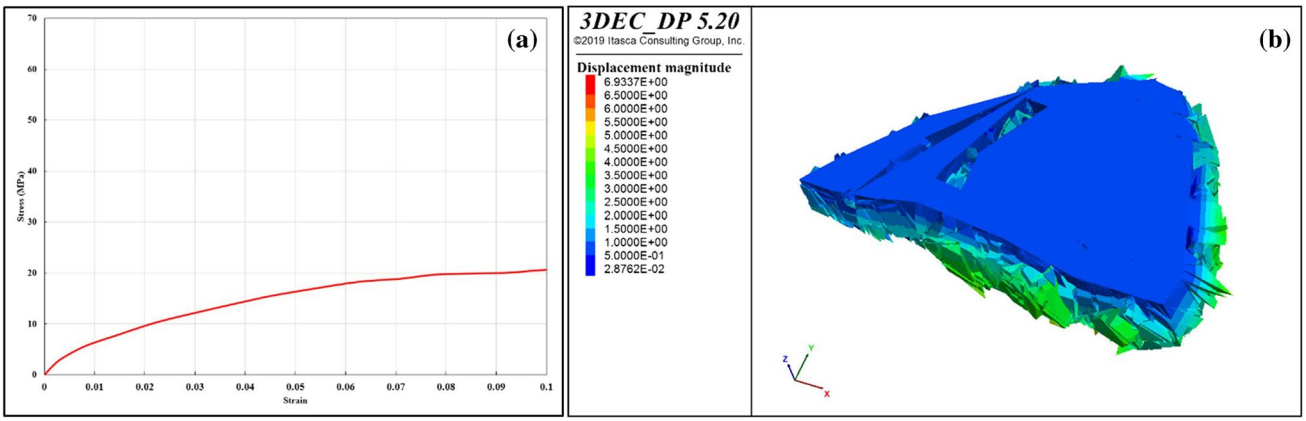

Fig. 6 **a** Stress vs strain plot for Mohr–Coulomb pillar model (left); **b** displacement magnitude and deterioration of the Mohr–Coulomb pillar model at its strength (right)

3 Estimating Stress Regime in FLAC-3D

The estimation of prevailing stresses in the pillars of an underground mine is a complex task. This research required estimating pillar stresses to understand if any modifications could be made to the pillar design, having already determined the pillar strength. The development of an appropriate numerical rock model is very important for simulating the excavation sequence and redistributed stresses in the mine pillars. Also, the numerical model needs to be first calibrated using field instrumentation data for correctly estimating the response of pillars to redistributed loading. This involves using suitable physico-mechanical rock properties. FLAC-3D was used for this sub-task involving numerical modeling and calibration of the mine model. To study the response of pillars to the redistributed stresses, a layout of the mine was modeled, and an excavation sequence was replicated to arrive at the current pillar layout. In this study, the rock mass properties are calibrated, and the redistributed stresses were determined using a suitable material model in FLAC-3D.

3.1 Model Generation and Boundary Conditions

The case study mine is situated in a region with middle- to lower-Ordovician-age, high-calcium limestone. The thickness of the orebody is about 30 m and dips at approximately 30° southeast as visible from the outcrop. Each level has an east and west section branching off the corkscrew ramp; at present, each branch contains a footwall and hanging wall tunnel separated by 24.5 m × 24.5 m × 30.5 m rectangular pillars left after complete extraction from the eventual stoping, and drives are approximately 8-m tall and 12.8-m wide. Figures 8a and b shows a schematic view of the FLAC-3D model with pillars and headings designed for the study. A simpler model was preferred for this sub-task since the exact

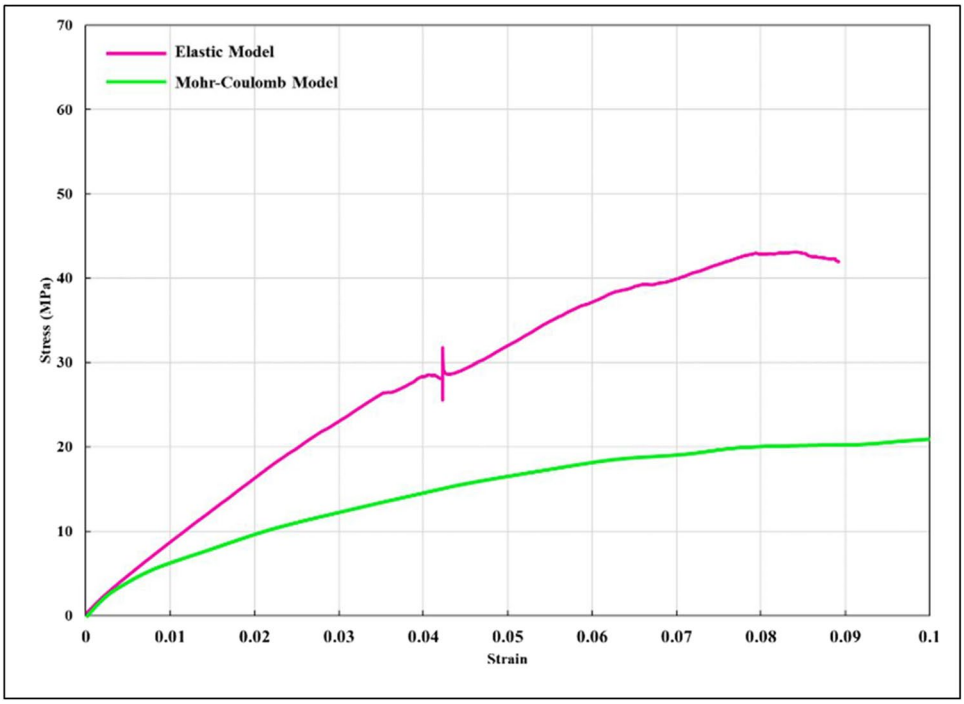

Fig. 7 Stress vs strain plot for Pillar-X for Elastic vs Mohr–Coulomb constitutive model

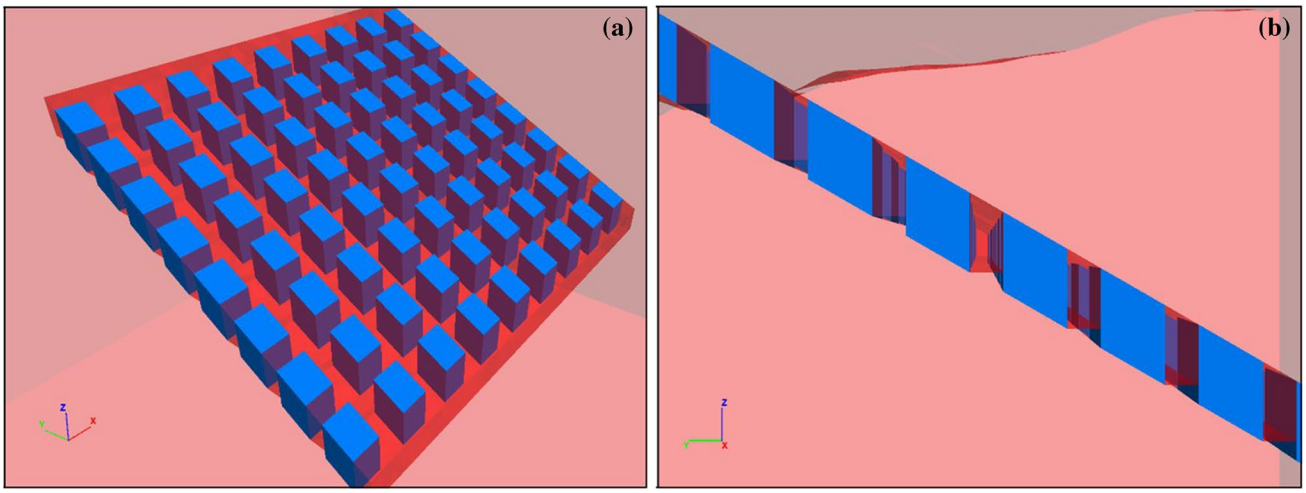

Fig. 8 **a** and **b** Different views of the ideal schematic layout of the case study mine

redistributed stress values cannot be measured using numerical modeling. Although the layout designed for this study was based on the ideal mine plan, it will provide a close estimate of how the stresses are redistributed after mining.

The model size was limited by artificial boundaries wide enough to prevent any influence of bounding sides on the mine excavations. The top face was kept free, and the bottom and four side faces were bound as shown in Fig. 9. The vertical and horizontal stress gradients were applied to the model as determined by the in-situ stress measurements by the mine operator. These measurements were done using the United States Bureau of Mines (USBM) Borehole Deformation Gage (BDG) borehole measurements.

3.2 Assigning Properties and Material Models in FLAC-3D

The physico-mechanical properties for the intact rock were measured by the mine management using laboratory testing of intact rock cores. Both the orebody and host rock are modeled as Mohr–Coulomb materials. A summary of all the intact rock parameters, namely, density, shear modulus, bulk

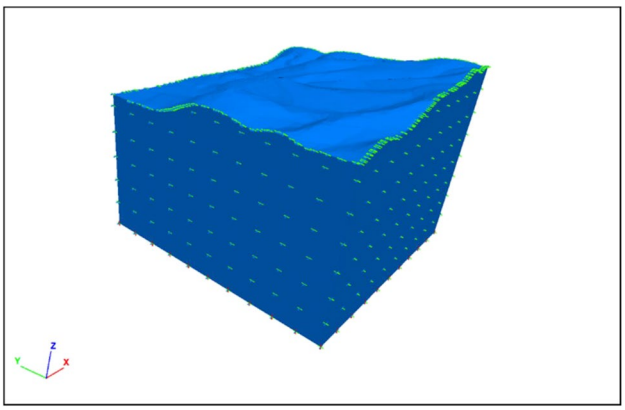

Fig. 9 FLAC-3D model extent with fixed boundaries marked by crosshairs and free topographic surface

Table 1 Summary of intact rock input parameters for stress estimation

Intact Rock Properties	Orebody	Hanging wall	Foot wall
Density, ρ	2690 kg/m^3	2691 kg/m^3	2722 kg/m^3
Bulk modulus, K	37.86 GPa	32.81 GPa	37.69 MPa
Shear modulus, G	20.57 GPa	25.64 GPa	25.18 MPa
Poisson's ratio, μ	0.27	0.19	0.21
Cohesion, c	12.53 MPa	6.50 MPa	17.34 MPa
Friction angle, Φ	36.73	52.13	37.69
Tensile strength	2.69 MPa	2.77 MPa	3.30 MPa

modulus, Poisson's ratio, cohesion, and angle of friction is provided in Table 1.

Although the above properties reflect the strength of the intact rock, simulating the model would not consider the presence of discontinuities inherent in the rock mass. The mapped joint network causes a reduction in the strength of the intact rock. To factor in this reduction, the material properties being used for FLAC-3D must be calibrated so that they mimic the rock mass. The calibration of the FLAC-3D model is explained in detail in the next section.

3.3 Calibration of FLAC-3D Model

Calibration of a numerical model is very important for replicating the evaluation of stresses and understanding the response of excavations to redistributed stress. Ideally, the numerical model needs to be calibrated using the field data of stress changes around the pillars of interest. Since the locations desired for taking the instrumentation data were not available due to the fieldwork time frame, the material properties of the rock mass used in FLAC-3D were calibrated using the numerically simulated full-size pillar in 3DEC. Since it is cardinal to assess the stresses in the pillars after the mining, a 24.5 m × 24.5 m × 30.5 m rectangular pillar model was simulated in 3DEC. The 3DEC model simulates the real-life joints as Discrete Fracture Network (DFN), along with the measured intact rock properties. The properties of the joints used in the 3DEC model are provided in Table 3. Details about the DFNs are explained in Section 4.4. Figures 10a and b display the behavior of the pillar in 3DEC and FLAC-3D, respectively.

The pillar model was simulated in both software to their peak strength. The rock mass properties for the FLAC-3D model were modified to mimic the 3DEC pillar model filled with discontinuities as displayed in the figure above. From the figures shown above, it may be observed that both the pillar models yield at the same strength and follow nearly the same stress–strain plot. Since 3DEC simulates blocks as discrete and deformable elements displacing along the discontinuities, the pillar model shows rock deterioration when tested for strength, whereas FLAC-3D treats the rock mass as a continuum without any joints; hence, no deterioration is observed. Also, the graph for the FLAC-3D model displays elastic behavior at low strains because all the pillar zones demonstrate the same strength with the application of load, but they follow the Mohr–Coulomb

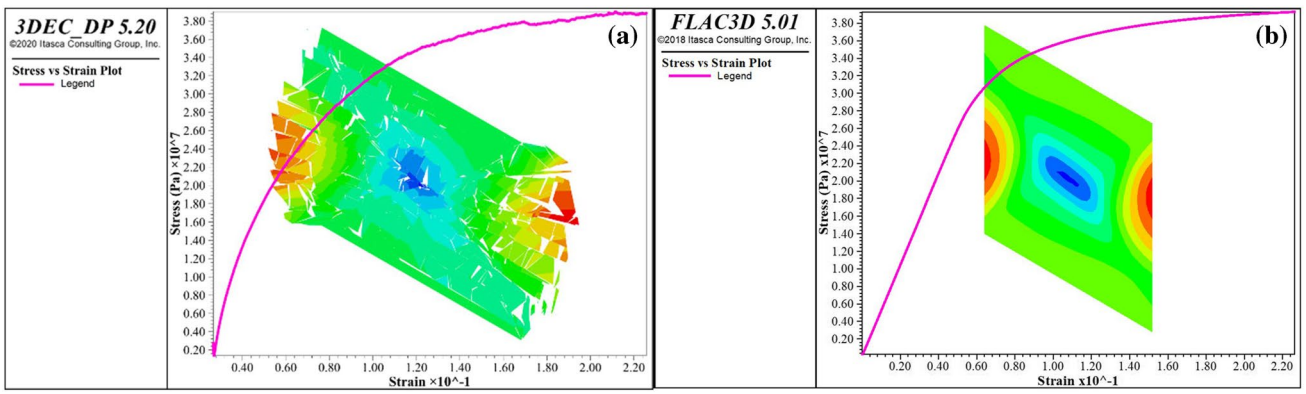

Fig. 10 Displacement contour and Stress–strain plot for **a** 3DEC model (left) and **b** FLAC-3D model (right)

Table 2 Summary of rock mass parameters for stress estimation in FLAC-3D

Rock Mass Properties	Orebody	Hanging wall	Foot wall
Density, ρ	2690 kg/m^3	2691 kg/m^3	2722 kg/m^3
Bulk modulus, K	378.6 MPa	328.1 MPa	376.9 MPa
Shear modulus, G	205.7 MPa	256.4 MPa	251.8 MPa
Poisson's ratio, μ	0.27	0.19	0.21
Cohesion, c	8.08 MPa	4.19 MPa	11.19 MPa
Friction angle, Φ	35.93	51.01	36.87
Tensile strength, τ	2.69 MPa	2.77 MPa	3.30 MPa

behavior near the pre-peak and the post-peak strains, whereas for 3DEC, the presence of joints starts affecting the model from the very beginning and the pillar zones display the Mohr–Coulomb behavior from the start. Similar to orebody intact rock, a similar calibration was achieved for the hanging wall and footwall rock types. Table 2 shows the calibrated rock mass properties that were finally used for simulating the FLAC-3D model for estimating the stresses in the pillars.

3.4 Stress Estimation Results

Figures 11a and b shows the contour of vertical stresses over the FLAC-3D model before and after mining, respectively. In reality, the mine layout has not been followed perfectly. Often changes were made due to short-term mine planning for countering ground control issues while encountering karst voids and other occasional instability due to wedge formations in the immediate roof. Despite following the ideal case scenario, the extraction ratio in the model is approximately close to the real-life scenario. Figures 12a and b shows the vertical stresses in the mine level where Pillar-X is located before excavation, whereas Fig. 13a and b shows the vertical stresses after mining, respectively. The relative location of Pillar-X is the same as the virtual pillar marked in Fig. 13b, and it is assumed that it is exposed to the same stresses as determined using the numerical model. From the figure, it can be observed that the stresses in the pillar vary between ~5 MPa around the periphery of the pillar to ~8 MPa at the core of the pillar.

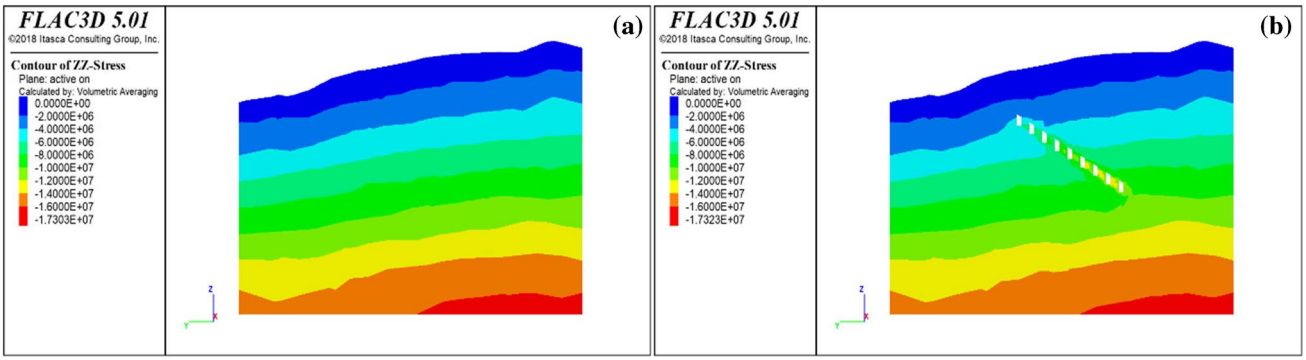

Fig. 11 **a** Contour of pre-mining ZZ-stress (left); **b** contour of post-mining ZZ-stress (right)

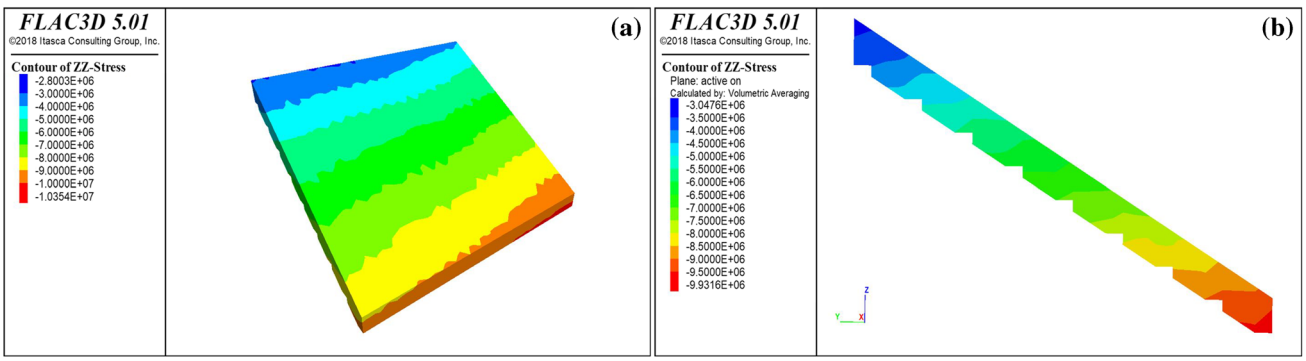

Fig. 12 **a** and **b** Perspective and cross-section view of the mine layout before excavation

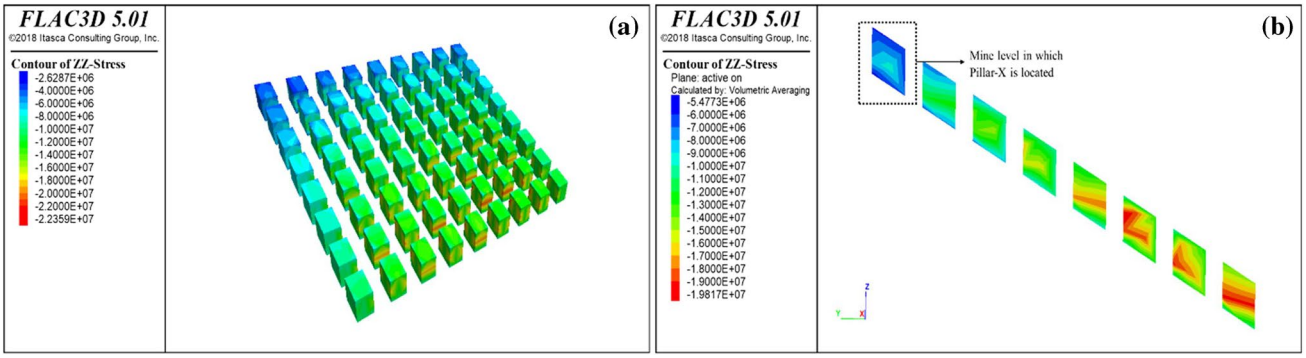

Fig. 13 **a** and **b** Perspective and cross-section view of the mine layout after mining

4 Numerical Modeling of Modified Pillar

After estimating the stress affecting Pillar-X, the numerical modeling tool is utilized to determine the optimum height to which it could be excavated or may have been designed. The software uses the distinct element method (DEM) for simulating the rock as a discontinuum media comprised of discrete blocks formed with joints and fractures. Similar to the previous study, this research sets individual blocks as deformable material which are meshed as finite different zones. The pillar strength is tested under increasing axial stress which leads to a movement along the joints and rotation of blocks.

4.1 Pillar-X Model Designs

For this study, the objective was to keep the pillar geometry constant but increase the height of the pillar by 10 ft for subsequent model design testing. It should be noted that the current height at which the pillar is 30 ft and was kept as a precautionary measure for the karst void discovered while the mine advances. However, no further study or ground control analysis was done by the mine planning team to estimate the optimum design of the pillar without compromising the local stability. In this study, pillar height was increased in the intervals of 10 ft (3.048 m) starting from the initial height of 50 ft (15.24 m). Three scenarios were tested for pillar models of height 50 ft, 60 ft, and 70 ft. Numerical modeling for pillar models for height above 70 ft was not carried out because the pillar model height of 70 ft and above did not meet the factor of safety criteria of 1.5 [9]. This is further discussed in detail in the results and analysis section. Figure 14 shows the pillar models with varying heights that were tested for pillar strength.

4.2 Physico-mechanical Properties

The physico-mechanical and geotechnical properties for the rock mass and joints used in the numerical model are tabulated in Table 3. As mentioned earlier, these properties are measured by the mine management using geotechnical borehole measurements and laboratory testing. The calculated values for joint shear stiffness and joint normal stiffness are based on the work performed by Bandis et al. [3]. Both the Elastic-Isotropic and the Mohr–Coulomb constitutive models were used to simulate rock behavior in the numerical model. It is believed that the Mohr–Coulomb model could be the ideal model to study the response of the rock mass, but the Elastic-Isotropic model state closely follows the karst cavity failure observed in the mine. For this reason, the study covers evaluating the pillar behavior concerning both the constitutive models. The discontinuities, however, are modeled using the Coulomb slip constitutive model to represent the physical response of rock joints.

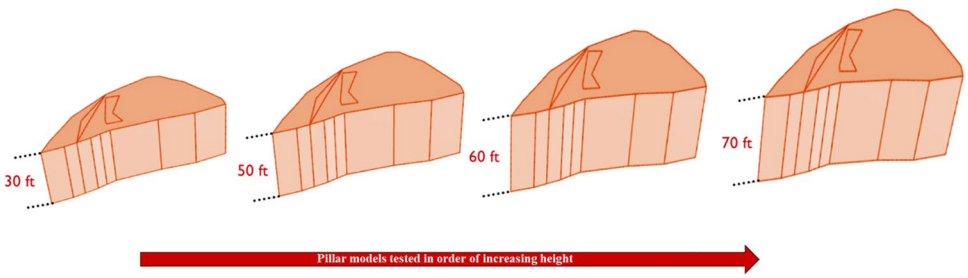

Fig. 14 Pillar-X model designs with varying heights tested for strength

Table 3 Physico-mechanical properties for intact rock and joints

Intact Rock Properties	
Density	2690 kg/m^3
Bulk modulus, K	37.86 GPa
Shear modulus, G	20.57 GPa
Poisson's ratio	0.27
Cohesion	12.53 MPa
Friction angle	36.73
Dilation angle	24.5
Joint Properties	
Joint normal stiffness	300 GPa/m
Joint shear stiffness	30 GPa/m
Joint friction angle	30^o
Joint cohesion	0.0

4.3 Boundary Conditions

Compressive stresses are applied axially along the vertical axis to the pillar. Since the pillar is not bounded on the sides, boundary conditions were kept free on the sides. Constant load application was initiated at the top and bottom of the pillar model using an applied velocity of about 0.5 µm/s [6]. It is assumed no horizontal movement is present at the top and bottom face of the pillar. Each numerical model was run until pillar model failure was observed for each height modification.

4.4 Discrete Fracture Network (DFN)

The use of a discrete fracture network in this study plays an important role in deciding the strength of the pillar models. Different parameters of the discontinuity network such as size information (trace length and area) and orientation information (dip, dip direction, and strike) were utilized in generating DFN using 3DEC. The details about the structural mapping in the case study mine and generating DFN using the statistical information provided in the previous study [16]. Figure 15 shows the pillar comprising of multiple blocks formed after being cut by the DFN to simulate a close representation of the geological structures in a rock mass.

5 Results and Analysis

The numerical modeling analysis for the two constitutive models (Elastic and Mohr–Coulomb) was performed to evaluate the performance of the pillar models with increasing load. The stress levels are plotted versus axial strain along the pillar to study the behavior of rock mass with increasing strain. The models were subjected to increasing axial stresses until yielding and ultimately failure is achieved. The criterion of failure is easy to identify in elastic rock mass by observing for a sudden drop in the stress values and looking at the deterioration levels of the pillar models. For Mohr–Coulomb models, however, the simulation is stopped until the stress vs strain plot line attenuates and no substantial increase in stress is observed with strain. Figures 16 through 18 show the different plots for pillar models of height 50 ft, 60 ft, and 70 ft for Elastic and Mohr–Coulomb model simulations. For all the simulated pillar models, it is observed that with an increase in compressive stress, tensile failures increase along the sidewall of the pillar leading to spalling. The pillar models fail upon reaching their ultimate strength with a subsequent increase in the compressive stresses. The karst void in every pillar model follows the same geometry. It is assumed that the karst volume extends in the roof and has the same height as a pillar model for equivalent comparison. From the study in FLAC-3D for estimating stresses in the mine and Pillar-X, it can be inferred that the stresses inside the pillar exist in the range of ~5–8 MPa. For further analysis, the highest value of 8 MPa is assumed to be the value of stress in Pillar-X. To maintain a Factor of Safety of 1.5 or higher, the pillar strength cannot fall below 12 MPa. The pillar models with larger heights will have a lower strength value compared to a model with a smaller height. Hence, pillar models with a subsequent increase in height of 10 ft were tested until the

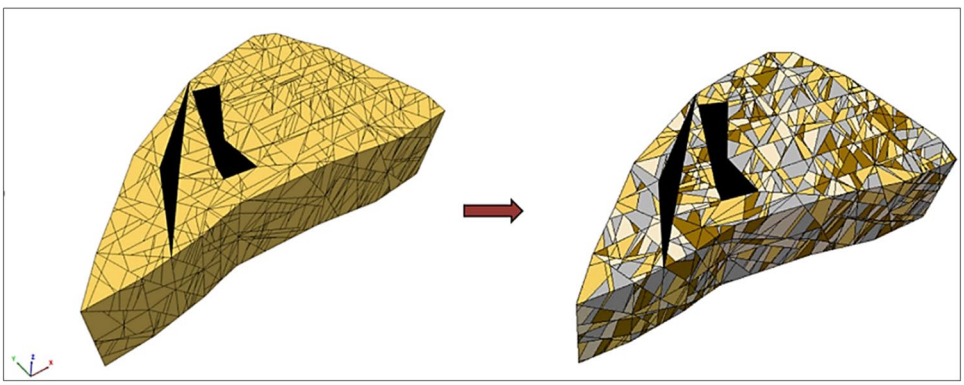

Fig. 15 Pillar-X with karsts represented using jointed blocks in the presence of a DFN

desired strength value is reached. The observations and their analyses are as follows:

A. *Elastic Constitutive Models*

For the models simulating Elastic rock mass with Coulomb-slip discontinuities, it is observed that all three models meet the factor of safety criteria. The strength of the Pillar-X model when extended to a height of 50 ft was found to be ~25 MPa and that of height 60 ft was ~20 MPa. When the height of the pillar model was extended to 70 ft, it yielded at ~12.5 MPa, just over the factor of safety value by a small margin. It was concluded that any further increase in height would lead to a pillar strength of less than 12 MPa; hence, no further simulations were carried out. An interesting observation was that the 50-ft and 60-ft height pillar models followed the same path on the Stress vs Strain plot when subjected up to a stress of 15 MPa or a strain value of 0.03. However, the same was not true for a pillar model with a height of 70 ft. It is inferred that with increasing pillar height, the number of discontinuities also increases by virtue of increased pillar volume. Hence, after a certain point, the constitutive properties of the joint network dominate the mechanical behavior of the overall intact rock (Figs. 16, 17, and 18).

B. *Mohr–Coulomb Constitutive Models*

For the models simulating Mohr-Coulomb rock mass behavior, it is observed that only the 50-ft-high model of Pillar-X meets the factor of safety criteria. The model yielded at a stress level of ~16.5 MPa. The pillar model

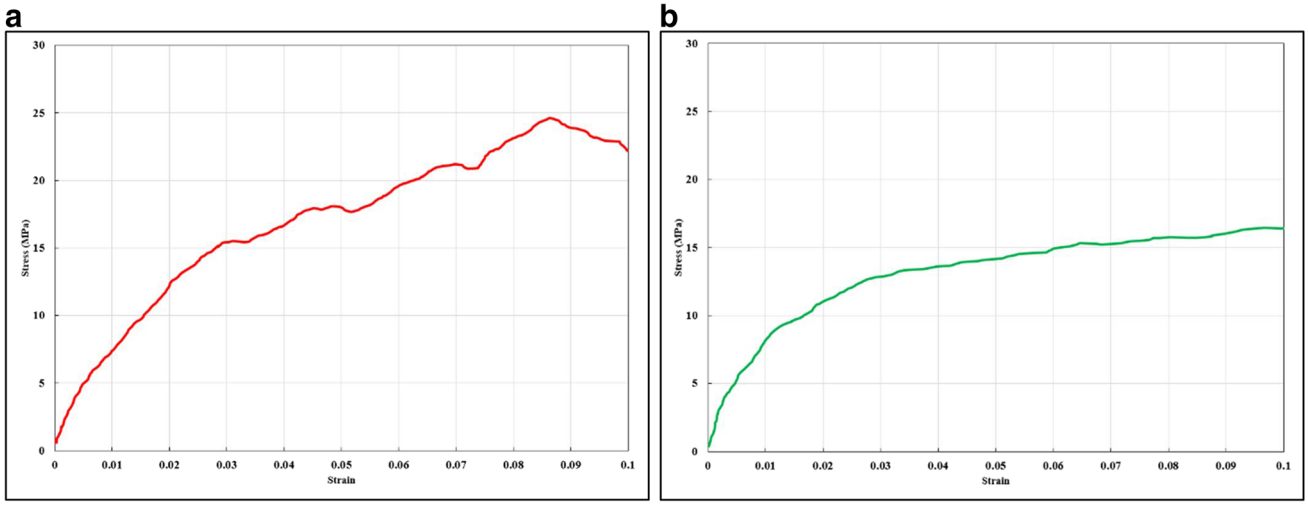

Fig. 16 (**a**) Stress vs strain plot for a 50-ft Elastic model. (**b**) Stress vs strain plot for a 50-ft Mohr–Coulomb model

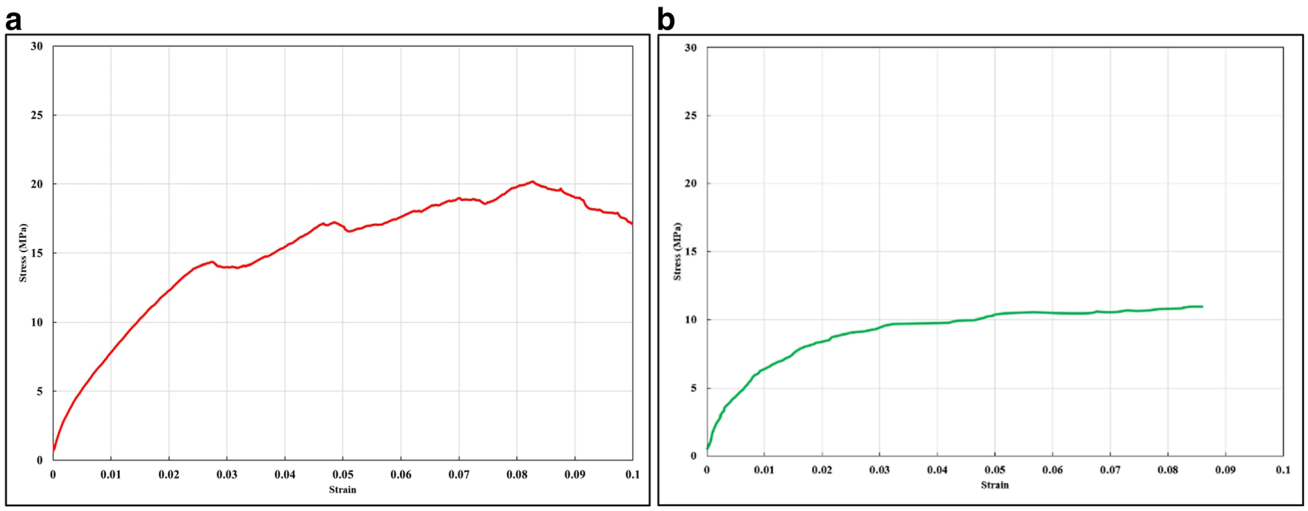

Fig. 17 (**a**) Stress vs strain plot for a 60-ft Elastic model. (**b**) Stress vs strain plot for a 60-ft Mohr–Coulomb model

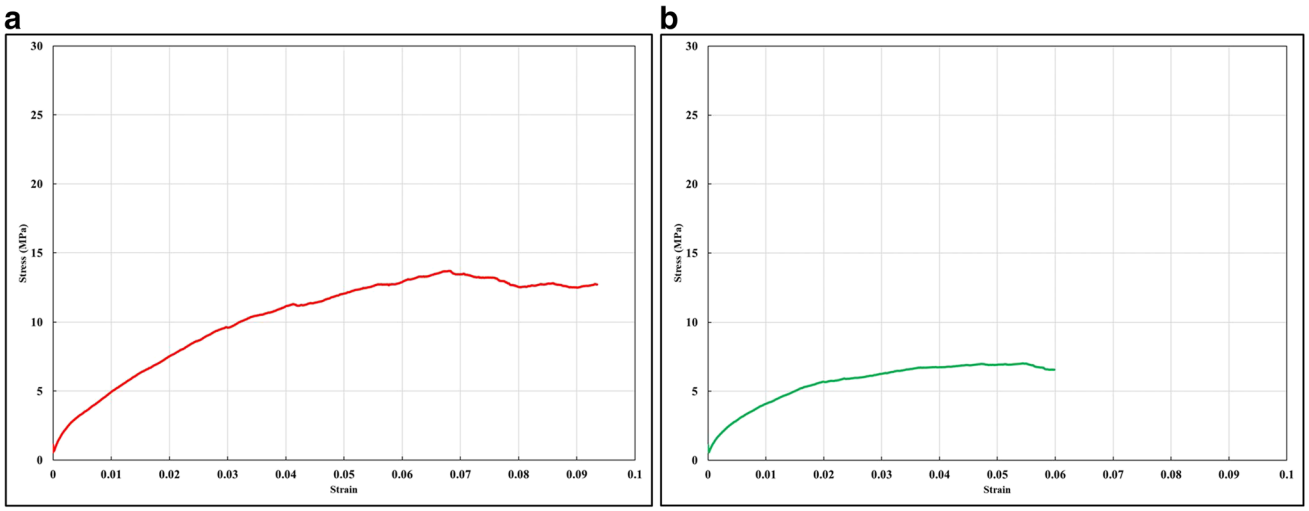

Fig. 18 (**a**) Stress vs strain plot for a 70-ft Elastic model. (**b**) Stress vs strain plot for a 70-ft Mohr–Coulomb model

with the height of 60 ft shows strength of about 11.5 MPa, just falling short of meeting the factor of safety criteria, whereas the 70-ft pillar model does not meet the criteria and fails at ~7 MPa. It can be observed that the Mohr-Coulomb pillar models show a considerable reduction in strength compared to the Elastic models. The pillar models tested in this scenario are simulating a perfectly plastic behavior of the rock mass. This has been done by implementing the dilation angle parameter in the inbuilt Mohr-Coulomb constitutive model in 3DEC. Furthermore, any intermediate heights for Pillar-X between 60 ft and 70 ft were not tested for this scenario as the 60-ft-tall pillar was almost on the boundary for meeting the factor of safety criteria and an increase in height was predicted not to meet the threshold value of 12 MPa (Figs. 16, 17 and 18).

C. *Variation in Pillar Strength with Height*

The pillar strength determined for various modified models for this study, plus the strength of the original pillar from the previous study were plotted against their height. The plot was constructed for both the Elastic and the Mohr-Coulomb pillar models. It may be observed that with an increase in height, the pillar strengths for both constitutive models approach towards each other. The data is not enough for predicting the approach of strengths towards a common point. However, at this stage, it may be predicted that as the height of the pillar model increases, the number of joints and fractures also increase manifold. Since the joint behavior is simulated using the Coulomb-slip model, the only difference in the two scenarios is the constitutive model for the intact rock. This may lead to a conclusion that the discontinuity features dominate the response of rock mass to stresses after a certain increase in the size of the pillar model. Figure 19 shows the variation in pillar strength for different heights for the Elastic and Mohr-Coulomb pillar models.

6 Conclusions

This paper studies the modification to the design of an underground stone pillar affected by the karst cavity. The modification is essential to understand the improvisation necessary to maintain stable design without compromising ore production. The primary aim is to tackle the instability issue in karst-ridden pillars and utilize numerical modeling to improve upon existing pillar design. Varying results are achieved when testing the strength of the Pillar-X model with a subsequent increase in height for each simulation. To understand the existing stress state of the pillar, numerical

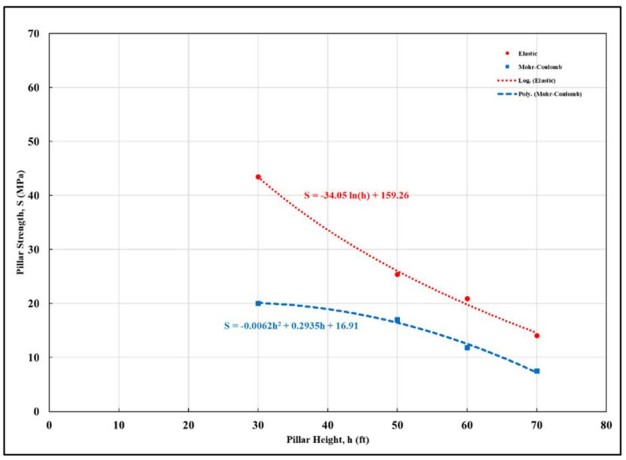

Fig. 19 Stress vs strain plot for a 60-ft Mohr–Coulomb model

modeling was performed by utilizing in situ stresses and excavation planned throughout the mine. This study serves as a secondary and concluding research for the preliminary study aimed at estimating the effect of karsts on Pillar-X strength [17]. The research is important for understanding the current stress regime and the response of pillars and excavated areas to any change in it, especially in a karst-affected area. This would help devise a good strategy for planning a secondary recovery from the pillars without jeopardizing the local or global stability. Some important conclusions that can be drawn from this study are:

- In the case study mine, ground control issues were encountered when mining advanced into a karst-affected pillar, also known as Pillar-X. To counter this problem, the mine management decided to alter the design and increase the size of the pillar as a means of the ground control measure.
- A preliminary study estimated that despite hosting the cavity, the pillar is capable of supporting higher stresses without causing local instability. This could be implemented by modifying the pillar design in terms of increasing its height and stoping it to the lower level.
- To understand a justifiable pillar design, existing stresses around and on the pillar were estimated by using modeling in FLAC-3D. Calibration of the in situ model was carried out and excavation sequencing was implemented to arrive at the current redistributed stress regime. It was estimated that the current stress state in the range of ~5–8 MPa could be acting on Pillar-X. Assuming a factor of safety value of 1.5, this would put a feasible pillar strength to be 12 MPa or above with a design modification.
- To assess the viable height increase, different models with the same pillar geometry but varying height were numerically simulated. The height was increased in intervals of 10 ft until the pillar model tested for a strength of 12 MPa or less. Axial stress was applied to the pillar models for numerically testing their strength in 3DEC. A discrete fracture network was also used to replicate the behavior close to real-world discontinuities.
- For pillar models with Elastic rock mass with Coulomb-slip joints, it was determined that the height of Pillar-X could be increased to 70 ft (21.34 m) while meeting the factor of safety criteria. The strength of the 70-ft pillar model was found to be ~12.5 MPa based on the stress vs strain plot. An interesting observation was that, unlike the 70-ft pillar, the 50 ft- and 60-ft pillar models followed the same curve on the stress vs strain plot up to a stress of ~15 MPa or a strain value of 0.03.
- For pillar models with Mohr–Coulomb rock mass with Coulomb-slip joints, only the 50-ft pillar model meets the factor of safety criteria yielding at a strength of ~16.5 MPa. In this case, the 60-ft model just fell short of meeting the criteria by testing at a strength of ~11.5 MPa. The behavior of rock mass in the underground stone mine skews towards the elastic rock mass criteria, but it is recommended to consider the Mohr–Coulomb constitutive model for numerical simulation after factoring in a conservative approach for a karst-affected mine.
- From the plot of pillar strength vs height for both the constitutive models (Elastic and Mohr–Coulomb), it may be observed that with an increase in height, the pillar strengths tend to approach towards the same magnitude. The data is considerably less for this prediction and more simulations are desirable. But, at this point, it may be inferred that with an increase in height, the number of discontinuities increases manifold, and their response takes over the behavior of intact rock mass to stresses.

Acknowledgements The authors would like to thank the National Institute for Occupational Safety and Health (NIOSH) for funding the project, and Dr. James Hazzard and Itasca Consulting Ltd. for their support and guidance during this study. Views expressed here are those of the authors and do not necessarily represent those of any funding source.

Funding This work is funded by the National Institute for Occupational Safety and Health (NIOSH) Mining Program under Contract No. 200–2016-91300.

Data availability Data subject to third party restrictions.

Code Availability Not applicable.

Declarations

Conflict of Interest The authors declare no competing interests.

References

1. Andriani GF, Parise M (2015) On the applicability of geomechanical models for carbonate rock masses interested by karst processes. Environ Earth Sci 74(12):7813–7821. https://doi.org/10.1007/S12665-015-4596-Z
2. Baggett JG (2019) A Study of Ground Penetrating Radar Methods in an Underground Stone Mine to Improve Ground Control [Virginia Tech]. https://vtechworks.lib.vt.edu/handle/10919/91393
3. Bandis SC, Lumsden AC, Barton NR (1983) Fundamentals of rock joint deformation. Int J Rock Mech Min Sci 20(6):249–268. https://doi.org/10.1016/0148-9062(83)90595-8
4. Bishop RE (2020) Applications of Close-Range Terrestrial 3D Photogrammetry to Improve Safety in Underground Stone Mines to Improve Safety in Underground Stone Mines. In Thesis. https://vtechworks.lib.vt.edu/handle/10919/98920
5. Bishop R, Monsalve J, Baggett J, Soni A, Ripepi N (2019) A comparison of laser scanning and photogrammetry in an underground limestone mine. 2019 SME Annual Conference and Expo and CMA 121st National Western Mining Conference, Preprint 19–095. https://doi.org/10.13140/RG.2.2.11354.16320
6. ISRM (1981) Rock characterization, testing and monitoring. ISRM suggested methods, 211

7. Caselle C, Bonetto S, Comina C, Stocco S (2020) GPR surveys for the prevention of karst risk in underground gypsum quarries. Tunnel Underground Space Technol 95:103137. https://doi.org/10.1016/J.TUST.2019.103137
8. Chen J (1988) Karst collapse in cities and mining areas, China. Environ Geol Water Sci 12(1):29–35
9. Esterhuizen GS, Dolinar DR, Ellenberger JL (2008) Pillar strength and design methodology for stone mines. In: Proceedings of the 27th International Conference on Ground Control in Mining. Morgantown WV: West Virginia University (pp 241–253)
10. Fazio NL, Perrotti M, Lollino P, Parise M, Vattano M, Madonia G, Di Maggio C (2017) A three-dimensional back-analysis of the collapse of an underground cavity in soft rocks. Eng Geol 228:301–311. https://doi.org/10.1016/J.ENGGEO.2017.08.014
11. Frisia S, Borsato A (2010) Chapter 6 Karst. Dev Sedimentol 61(8):269–318. https://doi.org/10.1016/S0070-4571(09)06106-8
12. Mark C, Gauna M (2017) Preventing roof fall fatalities during pillar recovery: A ground control success story. Int J Min Sci Technol 27(1):107–113. https://doi.org/10.1016/J.IJMST.2016.09.030
13. Monsalve JJ, Baggett JG, Soni A, Ripepi N, Hazzard J (2019) Stability analysis of an underground limestone mine using terrestrial laser scanning with stochastic discrete element modeling. In 53rd US Rock Mechanics/Geomechanics Symposium. OnePetro
14 Ninanya H, Guiguer N, Vargas EA, Nascimento G, Araujo E, Cazarin CL (2018) Analysis of water control in an underground mine under strong karst media influence (Vazante mine, Brazil). Hydrogeol J 26(7):2257–2282. https://doi.org/10.1007/S10040-018-1785-3
15. Parise M, Lollino P (2011) A preliminary analysis of failure mechanisms in karst and man-made underground caves in Southern Italy. Geomorphology 134(1–2):132–143. https://doi.org/10.1016/J.GEOMORPH.2011.06.008
16. Soni A, Monsalve JJ, Bishop R, Ripepi N, Baggett JG (2022) Estimating strength of pillars with Karst voids in a room-and-pillar limestone mine. Mining, Metallur Explor 39:1073–1086. https://doi.org/10.1007/s42461-022-00594-0
17. Soni A (2022) Optimizing Pillar Design for Improved Stability and Enhanced Production in Underground Stone Mines. Doctoral Dissertation. Virginia Tech. https://vtechworks.lib.vt.edu/handle/10919/110950